



Remote Sensing Capabilities of Detecting Spatio-Temporal Dynamics in Unregulated Gold Mining Hotspots in Ecuador

Inga Lammers¹, Christian Geiß^{2,3}, Jose Jara-Alvear⁴, Valerie Graw¹

¹Institute of Geography, Ruhr University Bochum (RUB), Germany

5 ² German Remote Sensing Data Center (DFD), German Aerospace Center (DLR), Wessling, Germany

³ Department of Geography, University of Bonn, Germany

⁴ Energy Sciences Research Group (CIENER), Universidad del Azuay (UDA), Cuenca, Ecuador

Correspondence to: Inga Lammers (inga.lammers@rub.de)

Abstract. Degradation of the Amazon rainforest is increasing by expanding human activities, especially unregulated gold mining. These pressures have intensified over the past decade due to rising global gold prices and policy shifts. Given the sensitivity of the topic and the need for transparent and reproducible information, this study assesses the suitability of remote sensing datasets, including Sentinel-1 (S-1) Synthetic Aperture Radar data, PlanetScope (PS) optical imagery, as well as the Satellite Embedding Dataset V1 (SED), for detecting unregulated mining and investigating the spatio-temporal dynamics of mining expansion. All datasets are processed mainly in Google Earth Engine with dataset-specific methodologies applied. Supervised quantitative classification approaches were used for the SED and PS imagery, covering the period from 2017 to 2024. For S-1 data, a Sequential Change Detection (SCD) approach was implemented. The analysis focuses on three mining hotspots in eastern Ecuador where unregulated activities have been reported. Results show a pronounced increase in mining extent and associated deforestation across all study areas, with particularly strong expansion during 2023 and 2024. Comparison of classification results indicates that persistent cloud cover and temporal inconsistencies limit the effectiveness of optical PS data, whereas the SED dataset provides a reliable and efficient alternative for annual assessments with minimal preprocessing requirements. The SCD analysis revealed detailed expansion dynamics, demonstrating that mining typically initiates along major rivers and progressively expands toward tributaries and surrounding forest areas. The multi-method approach further enables cross-validation of results, which are consistent with independent reports documenting similar spatial patterns and trends. The severe environmental consequences of unregulated mining and threats to communities emphasize the importance of systematic and transferable remote sensing-based monitoring frameworks to support environmental protection and enable timely, accessible reporting for environmental governance and decision-making.

1 Introduction

Although the Amazon rainforest covers only 0.5% of the Earth's surface, it hosts more than 10% of all plant and vertebrate species, making it the most species-rich subcontinental-scale ecosystem globally (Albert et al., 2023; Abramovay et al., 2021; Roy et al., 2018). It is also a critical component of the Earth system, contributing around 16% of global terrestrial photosynthetic productivity and regulating major carbon and water cycles. Despite this importance, the Amazon is increasingly



degraded by expanding human activities, including land-use change, hydrological alteration, and resource extractivism. These pressures contribute to an approaching ecological tipping point, with potentially severe consequences for biodiversity and climate regulation (Albert et al., 2023; Lenton et al., 2025; Flores et al., 2024).

35 In Ecuador, rich alluvial gold deposits have driven the expansion of mining activities. Policy changes, including the opening of ~13% of national territory to mining exploration in 2016, combined with rising gold prices and socio-economic pressures, have accelerated this development (Roy et al., 2018; Capparelli et al., 2021). A substantial share of this expansion is linked to unregulated or artisanal and small-scale gold mining (ASGM), which is typically characterized by low capital investment, labor-intensive methods, and limited regulatory oversight (Bank et al., 2014; Protschky et al., 2021). While ASGM provides
40 livelihoods, it is associated with severe environmental and health impacts. Mining-driven deforestation, river sedimentation, and pollution from toxic elements such as mercury have increased significantly, with deforestation linked to mining rising sharply in recent years (Borja et al., 2023; Mena-Quintana et al., 2025).

Given the dynamic and often short-term nature of mining activities, systematic monitoring is essential. It also provides technical support for decision making by governmental departments (Götze et al. 2016, Song et al. 2020). Remote sensing
45 (RS) has been applied to monitor mining sites in various ways. Often land use/cover changes have been identified using RS data, also time series data has been used to monitor changes related to mining around the world. While optical datasets are commonly used to monitor the extent and associated changes of mining sites, often with the help of spectral indices (e.g. Isidro et al. 2017, Lobo et al. 2018, Adamek et al. 2021). Synthetic Aperture Radar (SAR) technology is useful due to their independence of weather conditions and for monitoring in areas with more frequent cloud cover (e.g. Forkuor et al. 2020). For
50 underground mining SAR data can be used to observe land subsidence associated with mines by applying the Differential Interferometry SAR (DInSAR) technique to detect and monitor surface deformations (e.g. Sellers et al. 2022). Hyperspectral RS otherwise can be used to monitor vegetation health around mining sites (e.g. Zhang et al. 2012).

Due to the sensitivity of unregulated mining activities, this study relies exclusively on RS data to ensure both safety and objectivity. The analysis is based on freely or widely accessible datasets, including Sentinel-1 (S-1), PlanetScope (PS), and
55 Google's geospatial data repositories, and is implemented within Google Earth Engine (GEE), enabling a transparent, reproducible, and transferable workflow. Given the rapid expansion of unregulated mining and the limited availability of in-situ observations, satellite-based monitoring is essential for assessing associated environmental impacts such as deforestation, water pollution, and habitat fragmentation. Despite the increasing availability of earth observation data, there remains a lack of systematic evaluation of how different RS datasets perform in detecting and monitoring the temporal evolution of
60 unregulated mining activities. Existing studies often rely on a single sensor or approach, limiting the ability to assess trade-offs between spatial resolution, temporal frequency, and data accessibility. In particular, the question of which datasets are most suitable for specific monitoring objectives, and how their usability varies with user expertise, remains insufficiently addressed. Key parts of the study include (1) the identification and assessment of suitable RS-based datasets to detect unregulated gold mining activity and (2) to detect and quantify spatio-temporal patterns of unregulated mining in satellite time
65 series. In doing so, the study focuses not only on the detection of mining extent but also on understanding how mining sites



70 evolve spatially and temporally under varying observation conditions. By linking dataset characteristics to specific monitoring objectives and levels of technical complexity, this work seeks to provide a structured basis for selecting appropriate RS data in the context of unregulated mining. In addition, the study focuses on regions in the Ecuadorian Amazon where mining activities are either unregulated or occur outside formal concessions, contributing to improved understanding of spatio-temporal unregulated mining dynamics in areas where systematic information remains limited.

2 Study Area and Characteristics of Mining Sites

75 Ecuador is located in northwestern South America. Spanning 270,679 km², it includes both the Andean and Amazonian regions, and has a population of ~18.3 million, of whom ~750,000, including indigenous populations live in the Amazon (UNFPA, 2025; Villacis et al., 2012). Mining plays an increasingly important role, with 7,813 concessions covering 22,812 km² (9.2% of the mainland) as of 2021 (Peck et al., 2023). In addition, unregulated or non-compliant mining affected approximately 97.6 km² in 2026 (Amazon Mining Watch, 2026). Unregulated gold mining in Ecuador is predominantly alluvial and concentrated along river systems. Operations typically involve sediment excavation and mercury-based amalgamation, causing deforestation, soil erosion, river modification, and severe contamination of water and soils (Navas et al., 2010; Mora-Silva et al., 2021). These disturbances are clearly detectable in satellite imagery through features such as bare soil scars, water-filled pits, and altered river coloration.

80 This study focuses on three mining-affected areas in eastern Ecuador, located in the provinces of Napo, Orellana, and Zamora Chinchipe (further named: *Punino*, *South Napo*, and *Shaime*) (Fig. 1). Areas of interest (AOIs) were selected based on documented expansion of unregulated mining, primarily using reports from the Monitoring of the Andes Amazon Program (MAAP) and the Amazon Mining Watch. The selected AOIs cover a total of 121.32 km² and are further subdivided into smaller units to enable detailed analysis of spatio-temporal mining dynamics.

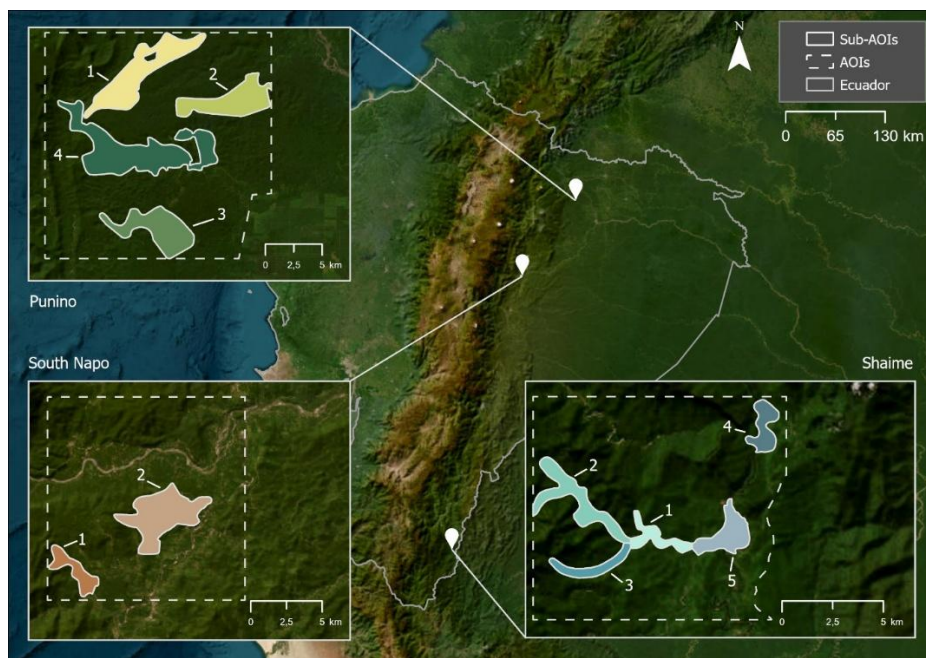


Fig. 1 Location of AOI's and Sub-AOI's within Ecuador. Sub-AOIs are color-coded and numbered for easier discrimination in the results.

With an area of roughly 89 km², *Punino* is the largest AOI. Located in northern Ecuador, it lies approximately 50 km south of the Colombian border and extends mainly across Orellana Province, with a smaller portion extending into Napo Province. The Rio Punino runs through the centre of the AOI, with tributaries such as the Rio Biguno and the Rio Acorna flowing into it. There are no major settlements within the AOI. The nearest city, Puerto Francisco de Orellana, is located approximately 20 km away. Since the early 2020s, there has been a dramatic increase in mining activity in this area, and rising tensions between miners and local residents have been reported (Plan V, 2024).

95 With a combined size of 14.13 km², *Shaime* lies in the province of Zamora Chinchipe in southern Ecuador, bordering Peru to the east. The Rio Shaime and the Rio Nangaritzza flow northwards through the region, while the Quebrada Shamataka flows in from the west. Smaller settlements located along the rivers are primarily inhabited by the indigenous Shuar people. As in other areas, gold mining provides an income for local workers and external suppliers of equipment and machinery. Tensions have arisen between miners and protestors, in a manner similar to that seen in Punino (Puertas 2018; Beltrán 2022).

100 The *South Napo* AOI covers 18.19 km² and is characterized by two major rivers: the Rio Jatunyacu, which flows west to east across the northern part of the area and the Rio Anzu, which runs northward from the south. Although the region is sparsely populated overall, it has the highest settlement density and anthropogenic modification among the three AOIs. In the southern part of the AOI lies the settlement of Carlos Julio Arosemena Tola.



3 Data and Methods

105 In this study, different methodologies and datasets are employed to detect and classify mining sites and to document their dynamics, depending on the specific characteristics of each dataset. Two main aspects are investigated: quantitative area classification and interannual spatial dynamics. To address these aspects, the study integrates three RS datasets: the Google Satellite Embedding V1 dataset (further: SED), PS, and S-1 data. All three datasets differ in their temporal and spatial resolution. Figure 2 illustrates how each dataset is used and outlines the corresponding methodological workflow. Together, 110 these datasets offer a comprehensive multi-temporal perspective on capturing both long-term trends and rapid dynamics, allowing for a detailed characterization of unregulated mining activity.

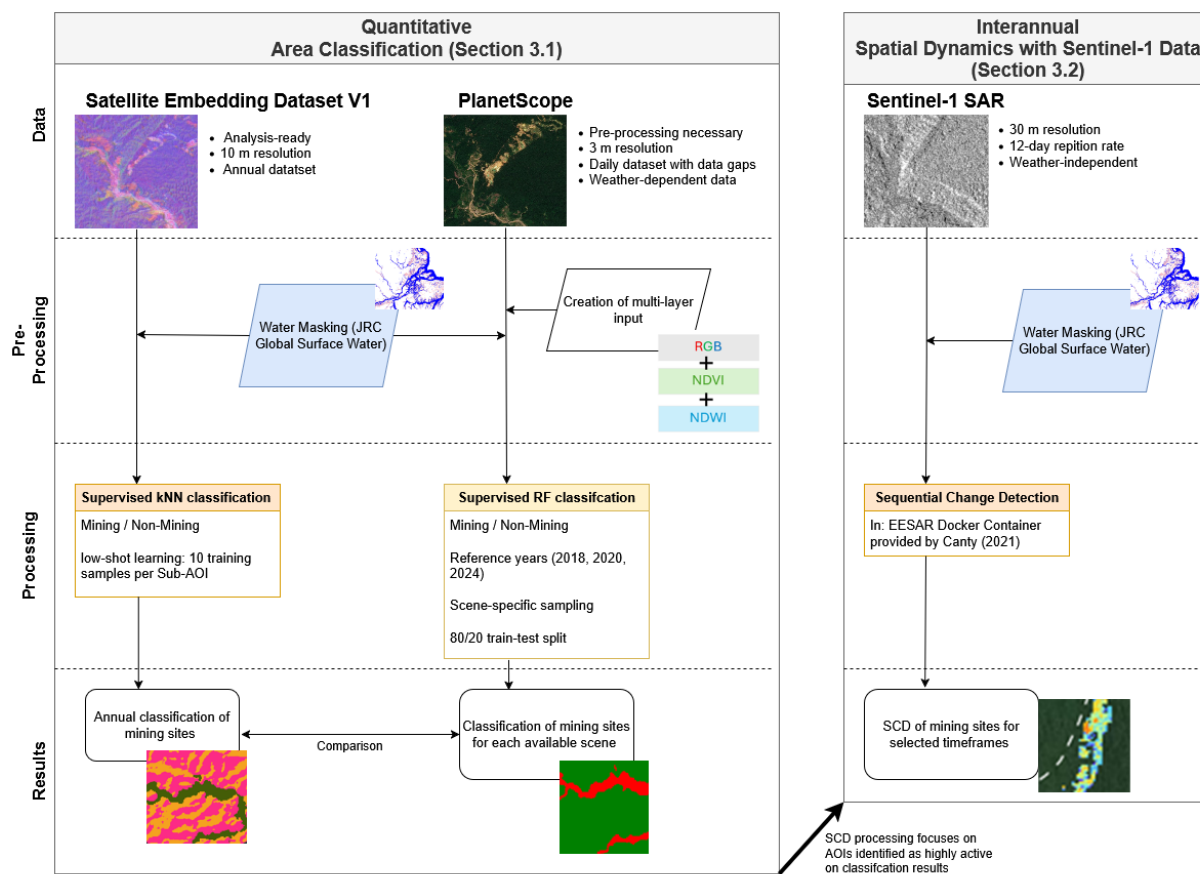


Fig. 2 Methodological Workflow

3.1 Quantitative Area Classification

115 3.1.1 Annual Quantitative Classification using the Google Satellite Embedding Dataset

The SED provides an analysis-ready 10 m dataset, that represents annual surface dynamics as 64-dimensional embedding vectors. These vectors are derived from the AlphaEarth Foundations Model and consist of multi-sensor data (optical, SAR,



LiDAR, and auxiliary sources). Its design removes the need for preprocessing and mitigates data gaps in tropical regions, making it well suited for large-scale analyses within GEE (Brown et al., 2025).

120 To generate an annual overview of mining-affected areas, a supervised classification approach was applied, as unsupervised clustering proved unreliable in AOIs with emerging mining activity. The embeddings support low-shot learning, meaning that even a small number of labeled samples (i.e. tens to hundreds of samples) can yield high-quality classifications. For each sub-AOI, a small number of training samples for both mining and non-mining areas were manually collected, which was sufficient for stable performance. Classification was performed using a k-nearest neighbors (kNN) algorithm within GEE’s Scalable
 125 Machine Learning for Earth Engine (SMILE) framework. Permanent water bodies were masked using the JRC Global Surface Water dataset by Pekel et al. 2016, which maps long-term surface water occurrence from multi-decadal Landsat observations. Despite partial underrepresentation in densely vegetated areas, it was retained for consistency. Training was guided by PS imagery from August 2024 to ensure accurate identification of active mining sites. The trained classifier was then applied to the full SED time series (2017–2024) to map the spatio-temporal evolution of mining activity across all AOIs.

130 3.1.2 Intermittent Quantitative Classification using PlanetScope Data

PS optical imagery was used to assess mining expansion over multi-year timescales using high-resolution observations acquired throughout each year. Sentinel-2 was initially considered, but persistent cloud cover limited its usability. In contrast, PS provides near-daily global coverage at 3 m spatial resolution, which results in more usable scenes for the analysis (Roy et al., 2021). Data were accessed via Planet’s Education and Research Program, downloaded from Planet Explorer, and processed
 135 in GEE. Only images with full AOI coverage and <1% cloud cover were retained and manually inspected, resulting in 431 usable scenes, with improved availability after 2020 (see Fig. 3).

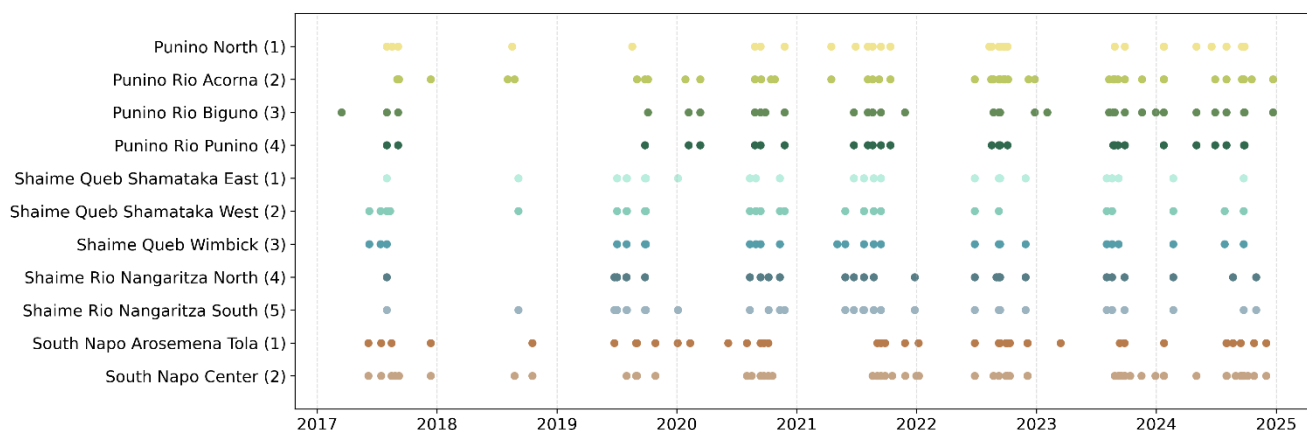


Fig. 3 PlanetScope data availability. Sub-AOIs are color-coded and numbered for easier discrimination in the results.

PS imagery was classified in GEE using a Random Forest (RF) classifier within the SMILE framework. RF is an ensemble
 140 learning method that constructs multiple decision trees from bootstrapped samples and aggregates their predictions, resulting



in robust and noise-resistant classification (Breiman, 2001). RF has been widely used for deforestation mapping applications (e.g. Grinand et al., 2013; Phan et al., 2020). To account for interannual variability in image characteristics, three reference images (2018, 2020, 2024) were used for training, which improved classification stability across the time series.

In addition to RGB and NIR bands, two spectral indices were included. The Normalized Difference Vegetation Index (see Eq. 1) exploits the contrast between red and near-infrared reflectance of vegetation and was used to distinguish vegetated areas from bare or disturbed mining surfaces (Rouse et al., 1974).

$$NDVI = \frac{(NIR - Red)}{(NIR + Red)}$$

The Normalized Difference Water Index (see Eq. 2) enhances open water features using the green and NIR bands and was used to identify water bodies and mining-related features such as sediment ponds and disturbed river margins (McFeeters, 1996).

$$NDWI = \frac{(Green - NIR)}{(Green + NIR)}$$

These variables were combined into a multi-layer input stack to provided more stable and accurate results.

Permanent water bodies were masked using the JRC Global Surface Water dataset, despite partial underrepresentation in densely vegetated river systems. Two classes (mining and non-mining) were defined, and training samples were manually collected for each image, with sample size adapted to scene complexity. The dataset was split into training and validation subsets, and the RF model was applied to all images from 2017 to 2024 to derive subregional mining extent and temporal dynamics.

3.2 Interannual Spatial Dynamics with Sentinel-1 Data

S-1 SAR imagery was incorporated within a SCD framework to capture short-term mining dynamics. Unlike optical data, SAR provides consistent observations independent of weather and illumination conditions, making it particularly suitable for persistently cloud-covered regions. Level-1 Ground Range Detected (GRD) products with 30 m spatial resolution and ~12-day revisit time were used (Geudtner et al., 2014). The SCD approach enables the detection of rapid changes, such as sudden expansion or relocation of mining activity, which are often not resolved in optical time series. It has been successfully applied in similar contexts to monitor dynamic landscape changes under frequent cloud cover (e.g. Asokan & Anitha, 2019; Graw et al., 2022). In this study, SCD was implemented following Conradsen et al. (2016) and Canty et al. (2020), using the EESAR Docker container provided by (Canty, 2021) in combination with processing in GEE. The algorithm evaluates multi-temporal SAR observations on a per-pixel basis, deriving statistical test values and corresponding p-values to identify significant changes across the time series. A significance threshold of 0.01 was applied to generate change maps, with the cmap option used to emphasize recent changes. To reduce false detections, permanent water bodies were masked using the JRC Global Surface Water dataset, acknowledging limitations in densely vegetated river systems.



4. Results

During the analysis, it was possible to identify different dynamics for each dataset due to the varying temporal and spatial resolution. The increase or decrease in mining areas is described and analyzed below. First, the results of the dataset with the coarsest temporal resolution are described, in this case the results of the SED. Then the results from the PS data are looked at and compared to the SED results. Finally, for areas and timeframes with high activity levels, the SCD is applied to further analyze these dynamics.

4.1 Annual Extent of Unregulated Mining Based on SED Classification Results

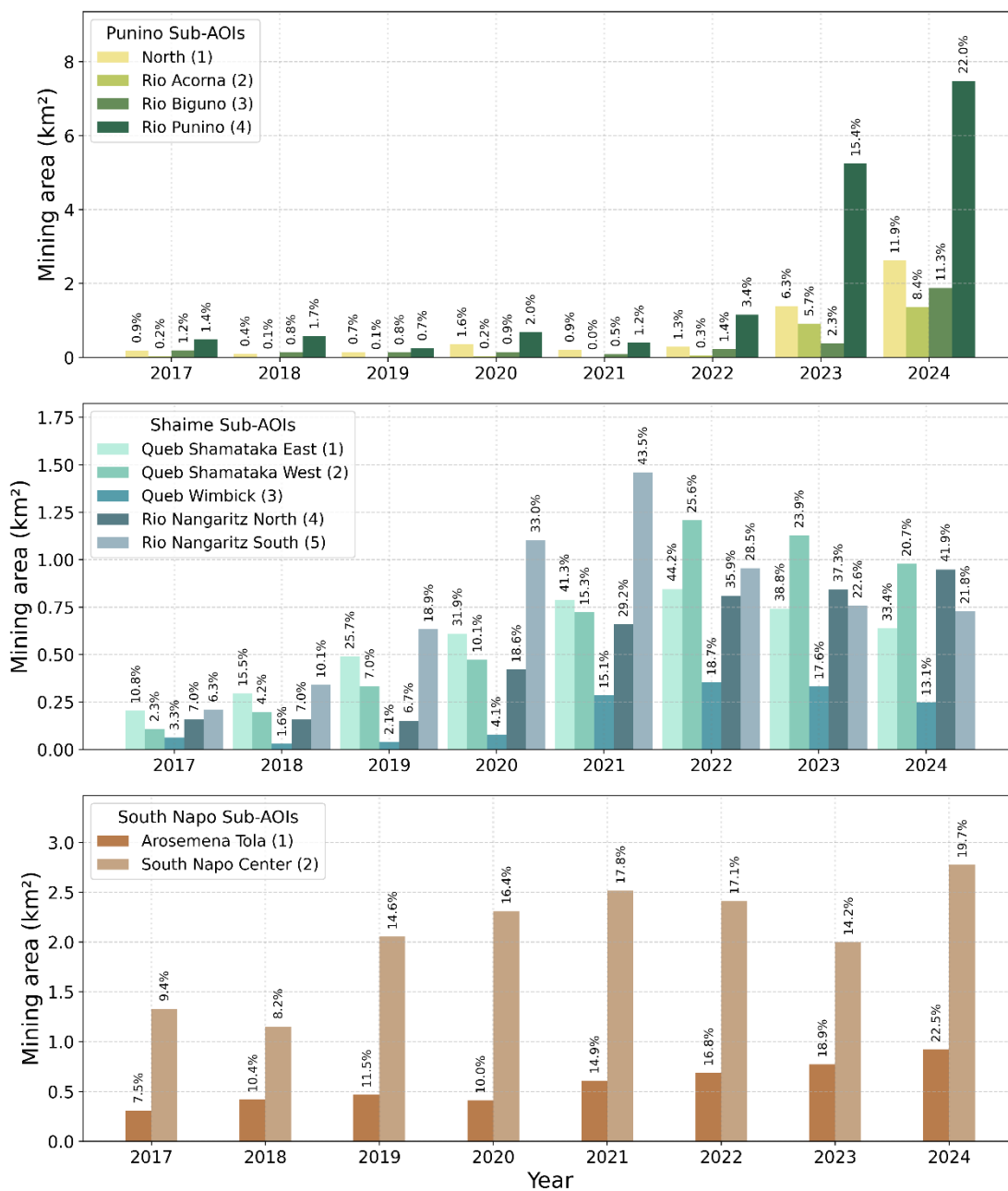
Across all analyzed AOIs, SED-derived mining extents reveal clear but regionally distinct expansion dynamics between 2017 and 2024 (see Fig. 4).

180 In the *Punino* AOI, mining activity remained low and spatially limited until 2022, which was then followed by a rapid expansion of mining sites in all subregions from 2023 onward. The Sub-AOI of *Rio Punino* emerged as a dominant hotspot, while other subregions followed similar but less pronounced trajectories.

The *Shaima* AOI exhibits more heterogenous dynamics, however all subregions experienced net growth over the study period.

185 The *Shamataka* subregions and Sub-AOI *Rio Nangaritza North* experience a steadily increasing extent in mining area, while *Wimbick* and *Rio Nangaritza South* are characterized by peak-and-decline behavior.

In *South Napo*, mining increased gradually in both subregions, exhibiting only short-term fluctuations. Compared to *Arosemena Tola*, *South Napo Center* maintained consistently higher activity levels throughout the study period.



190 Fig. 4 Results for SED-based classification. Percentages indicate the proportion of the AOI affected by mining.

4.2 Extent of Unregulated Mining Based on PlanetScope Classification Results and Comparison with SED Results

The PS-based classification for the *Punino* AOI reveals consistent temporal trajectories of mining expansion across all subregions despite data gaps in earlier years (Fig. 5). Patterns closely align with SED results, though PS generally captures



195 higher mining extents. Mining remains minimal until mid-2023, followed by rapid and synchronous expansion *across Punino North, Rio Acorna, and Rio Biguno*, mirroring the SED-derived shift. In contrast, *Rio Punino* shows earlier onset and substantially stronger growth, with both datasets capturing the pattern but PS indicating higher peak extents.

In the *Shaime AOI*, PS data indicate widespread intensification between 2017 and 2024 (Fig. 5). Trends closely match SED results, confirming a coherent temporal signal. However, PS reveals that expansion occurs in multiple short-lived phases, highlighting intra-annual variability not resolved in the annual SED data. This pattern is consistent across subregions, with
200 earlier and stronger intensification in *Rio Nangaritza South* and more gradual but continuous growth elsewhere.

For the *South Napo AOI*, both datasets show sustained expansion from initially low activity before 2019 to more extensive and persistent mining thereafter (Fig. 5). While *South Napo Center* exhibits earlier and stronger growth, *Arosemena Tola* follows a similar but more gradual trajectory.

Overall, PS confirms SED-derived trends while refining their temporal structure. However, direct comparison is constrained
205 by differing temporal and spatial resolutions. In some cases, the effect is more pronounced, as is evident in 2024 in the *Punino AOI*, where PS consistently indicates larger extents than SED. This suggests a systematic divergence that may reflect PS's higher sensitivity to small-scale features and SED's potential underestimation due to temporal aggregation and smoothing.

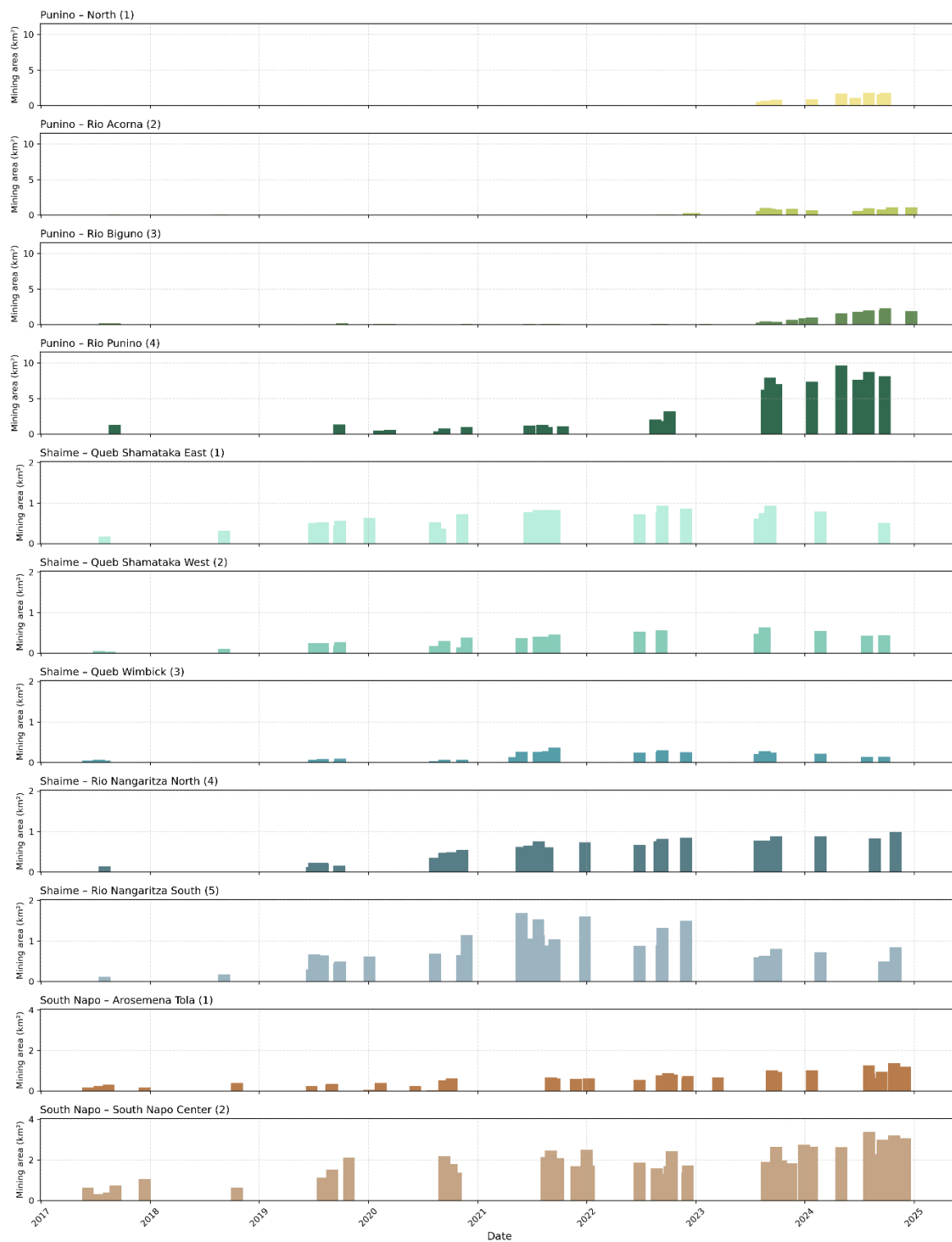


Fig. 5 Results for PS-based classification. Percentages indicate the proportion of the AOI affected by mining.



210 4.3 Interannual Dynamics- Sequential Change Detection Results for specific Regions/Timeframes

Analysis of the SED and PS results indicates that several AOIs experienced phases of rapid mining expansion, ranging from gradual development to abrupt increases. However, optical data alone does not fully resolve the temporal evolution of these phases due to frequent cloud coverage. This is particularly relevant for fast increases in mining extent, as seen in the *Punino* AOI. Therefore, SCD was applied to its four subregions, focusing on the year of strongest expansion (with both 2023 and 2024 analyzed for *Rio Punino*) (see Fig. 6).

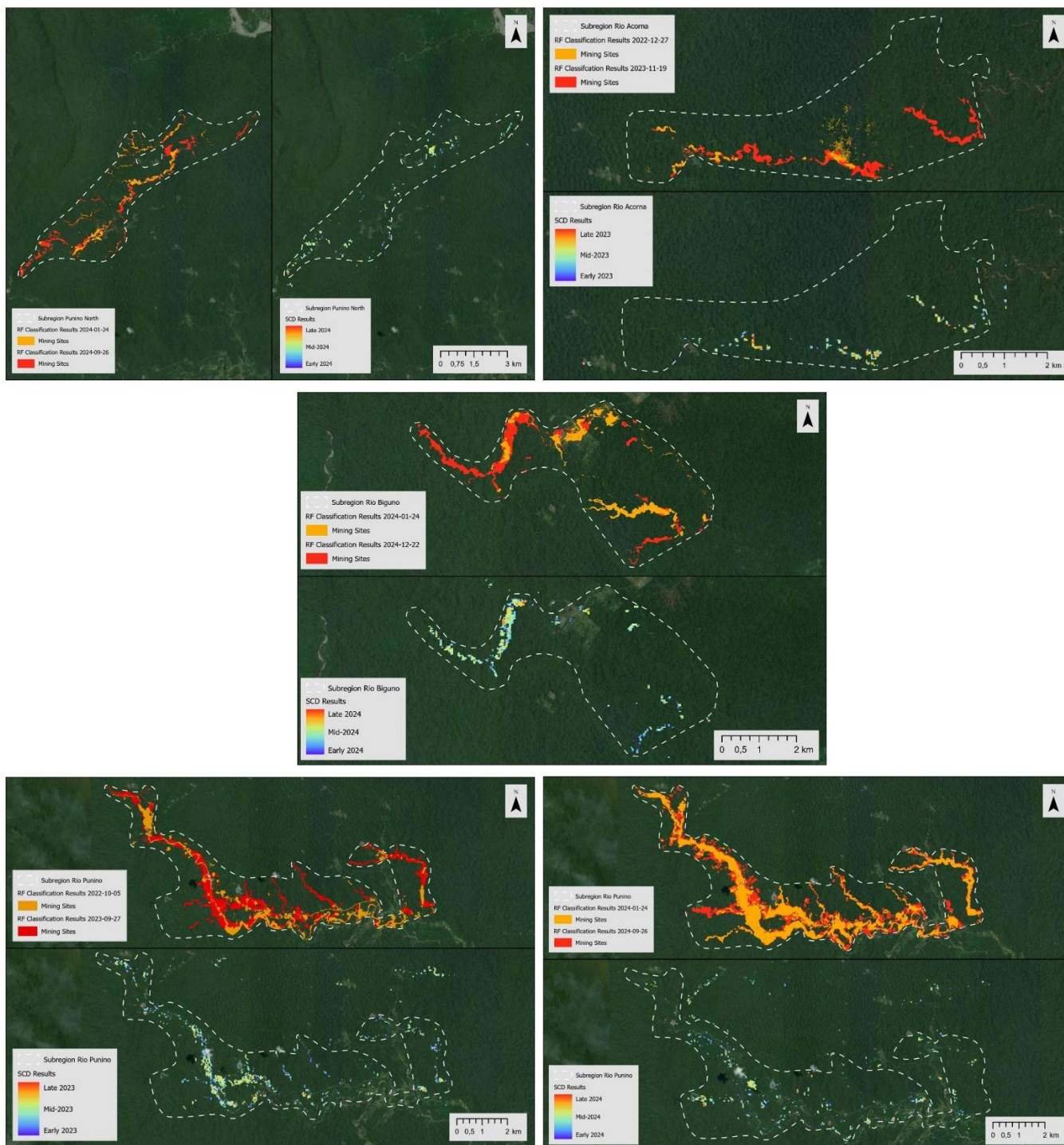
215 For *Punino North*, SCD results show a clear spatial progression of mining expansion along the central axis, extending toward the northeastern and southwestern margins. The coexistence of early-, mid-, and late-year detections indicates continuous activity throughout 2024, while localized early detections in the southeast suggest temporally limited clearing. Newly established sites in the north further indicate expansion into previously undisturbed areas. As in the other subregions, areas already classified as active mining sites show little to no change signal, reflecting the method's sensitivity to newly occurring land-cover transitions.

220 In *Rio Acorna*, SCD detections align closely with newly identified mining areas in PS imagery and follow linear patterns along established corridors. The SCD sequence indicates that changes in the westernmost patch occurred mainly during early 2023, whereas adjacent areas show activity emerging later in the year. Additional clusters exhibit detections throughout 2023, indicating sustained expansion rather than isolated events.

225 For *Rio Biguno*, change detections similarly correspond to newly disturbed areas and follow existing mining corridors. Continuous signals from early to late 2024 indicate sustained expansion, while localized clusters reflect shorter-term clearing phases. As observed elsewhere, pre-existing mining areas show minimal change signal in the SCD results.

230 In *Rio Punino*, SCD captures extensive expansion in both 2023 and 2024. In 2023, changes form spatially continuous corridors along river systems, indicating rapid, directed expansion. In contrast, in 2024, there are more dispersed and fragmented patterns, suggesting a shift toward expansion into surrounding areas and river tributaries.

Overall, SCD results confirm the spatial patterns observed in PS classifications while providing detailed insight into the timing and progression of mining expansion at sub-annual scales.



235

Fig. 6 Comparison of SCD results (right) with RF classification results based on PS data (left) for each Sub-AOI of the Punino AOI



5. Discussion

The three AOIs exhibit distinct dynamics of unregulated gold mining, reflecting different controls of economic drivers, accessibility, and local constraints. In *Punino*, for example, the rapid expansion of mining since 2023 indicates a strong
240 response to rising gold prices. This shows that previously unexploited areas can quickly become lucrative under favorable market conditions. In addition, the progression from the main river into tributaries illustrates how rapidly miners exploit resources. Due to the dense rainforest, no roads are visible in the satellite imagery. However, the rapid clearing suggests the presence of either a large workforce or substantial machinery for deforestation and mining.

In contrast, the heterogeneous trends in *Shaime* imply a stronger influence of local factors. Declining or stagnating mining
245 extents after peak activity may indicate resource depletion, reduced profitability, or social and regulatory pressures, while continued growth in *Nangaritza North* shows that these constraints are not uniform.

South Napo shows more moderate and temporally variable dynamics, suggesting either stronger limiting factors or a slower development trajectory. The delayed surge in 2024 indicates that mining expansion can occur in pulses, potentially triggered by changing economic conditions or possible spillover effects from other regions.

250 Overall, these results demonstrate that RS-based change detection captures not only the extent but can also be utilized to analyze the underlying dynamics of mining expansion in remote tropical regions.

5.1 Validation

The findings of this study align with reports by the Monitoring of the Andes Amazon Program (MAAP), which documents mining expansion, deforestation, and land-use change across the Amazon. In the *Punino* AOI, MAAP reports extensive mining
255 largely outside legal concessions, including within protected areas such as Sumaco-Napo Galeras National Park and Kichwa Indigenous territories (MAAP, 2024). In the *Shaime* AOI, mining occurs partly outside concessions or using unauthorized methods, particularly in ecologically important corridors like the Nangaritza River High Basin Protective Forest (Villa et al., 2022). *South Napo* shows similar trends, though with a smaller proportion of activity outside the official cadaster (MAAP, 2025).

260 In addition to MAAP, we compared our results with the Amazon Mining Watch (AMW) platform, an initiative led by the Amazon Conservation Association, Earth Genome, and the Pulitzer Center's Rainforest Investigations Network. AMW uses satellite imagery and AI to detect and map mining activity across the Amazon Basin, producing cumulative quarterly detections from 2018 onwards (Amazon Mining Watch, 2026). Across all three AOIs, strong spatial correspondence between the mining extents identified in this study and those reported by AMW are observed, supporting the robustness of the classification
265 framework. The convergence of independently developed methodologies, each using distinct data processing and classification strategies, increases confidence in the reliability of observed trends. However, notable differences exist. AMW outputs are comparatively spatially coarse, representing mining-affected areas with larger, generalized polygons. In contrast, the SED and PS-based classifications in this study delineate mining sites with higher spatial precision, closely following the outlines of



270 disturbed areas. This higher precision is further enhanced by incorporating a permanent water mask, which reduces false
detections along rivers and water bodies. Some discrepancies between datasets can therefore be attributed to differences in
spatial resolution, classification thresholds, and post-processing choices.

A detailed comparison for 2024 (Fig. 7) illustrates these differences at the sub-AOI level. In the *Punino* AOI, particularly in
Rio Acorna, AMW detected only a limited mining area, while SED classified mining activity across much of the subregion.
275 Similar patterns were observed in two western *Shaime* Sub-AOIs, where AMW outputs underrepresented smaller or newly
established sites. Despite these localized discrepancies, most areas show substantial spatial overlap, confirming that both
approaches capture the core mining expansion patterns.

From a monitoring perspective, these findings highlight the complementary strengths of multiple methodological approaches
for mapping ASGM landscapes. The AMW platform provides a standardized overview that is particularly valuable for large-
scale monitoring and interregional comparisons. In contrast, the SED and PS classification approaches enable a more detailed
280 delineation of mining features. Building on this, the SCD approach further refines the analysis by identifying consistent spatio-
temporal changes, thereby supporting the detection of progressive expansion dynamics rather than static extents alone.

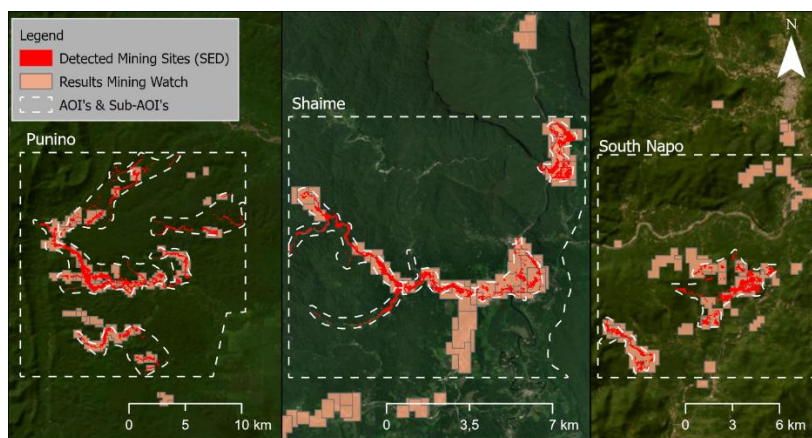


Fig. 7 Comparison of SED-based classification results and areas detected by Amazon Mining Watch

5.2 Contribution of Extractivism-Driven Deforestation to the Amazon Rainforest Tipping Point

285 The primary regional-scale drivers of the Amazonian habitat degradation include land-use change, hydrological alteration, and
climate-induced aridification, all of which interact to destabilize the forest–rainfall feedback system that sustains the Amazon.
As approximately half of regional precipitation is recycled through evapotranspiration, continued forest loss increases the risk
of a critical transition from a forested to a non-forested state, with a wide range of consequences. (Berenguer et al., 2021;
Wunderling et al., 2021; Cooper et al. 2020).

290 While large-scale agriculture remains the dominant driver of deforestation (Ferrante & Fearnside 2022), the results of this
study demonstrate that resource extractivism can act as a rapid and spatially targeted catalyst of forest loss. In particular, the
observed river-centered expansion of mining in the *Punino* AOI highlights how extractive activities penetrate previously



inaccessible regions, following waterways and subsequently expanding into tributaries. These dynamics indicate that mining can initiate new deforestation frontiers, potentially facilitating further land-use change. The intense landscape alterations that are caused, as well as the introduction of toxic substances into the soil and water systems create a condition that makes forest restoration measures even more complicated and harmful for humans carrying out restoration measures.

These findings underline the importance of RS-based approaches, as they enable the timely detection of rapidly emerging extractive hotspots in remote regions. Consequently, extractivism-driven deforestation should be considered not only as a secondary driver, but as a significant and dynamic contributor to processes that may push the Amazon rainforest closer to a tipping point.

5.2 Challenges, Limitations and Advantages of the Different Datasets

The analysis faced challenges due to differences in sensor characteristics and dataset properties, which complicate direct comparisons but also highlight the complementary strengths of each approach.

The SED dataset, provided as an annual 10 m product, requires no preprocessing, enabling rapid mapping and visualization of mining-affected areas and making it accessible to users with limited RS-data processing expertise. Its coarser resolution, however, limits the detection of small-scale features, and the aggregation of spectrally similar surfaces can lead to misclassification. In addition, AI-generated embeddings may vary in input data across years, although in this study no systematic temporal inconsistencies were observed. SED is therefore best suited for providing broad overviews of mining sites and their long-term evolution.

PS imagery offers higher spatial resolution (3 m) and the potential for finer temporal analysis. Image availability, however, is affected by cloud cover, satellite coverage, and scene quality. Spectral variability necessitated the use of multiple reference years for training, increasing computational demands. While PS-based classifications occasionally show abrupt changes, the higher resolution allows precise delineation of mining features and is valuable for validation and detailed spatial analyses.

SAR-based monitoring using the SCD approach provides near-continuous observations independent of weather, with a ~12-day revisit interval. This method effectively detects rapid deforestation associated with mining expansion, showing high correspondence with optical datasets. However, changes within previously deforested areas are often undetectable, limiting SCD to identifying newly occurring land-cover transitions. The 30 m resolution also constrains detection of fine-scale features. However, this dataset is best suited to continuously observe spatio-temporal dynamics of mining sites.

Across all datasets, deforestation linked to mining expansion was consistently observed. The absence of visible road networks suggests additional clearing under dense canopy, implying potential underestimation of total biomass loss. ESA's upcoming BIOMASS mission may provide improved detection of sub-canopy disturbances and a more complete assessment of the environmental impacts of unregulated gold mining.

While the methods capture mining extent and associated deforestation dynamics, they do not quantify broader ecological or social impacts. Unregulated gold mining often involves mercury amalgamation, releasing toxic elements into soils, rivers, and the atmosphere, which can bioaccumulate and pose risks to ecosystems and human health (Esdaile & Chalker, 2018; Gibb &



O’Leary, 2014). Although the present study can indicate areas with a heightened potential for mercury exposure based on mining-related land-use change, a comprehensive assessment of ecological and societal impacts requires additional investigations. In particular, in-situ measurements, long-term monitoring, and interdisciplinary studies are necessary to quantify contaminant pathways, exposure levels, and associated risks to affected populations.

330 6. Conclusion

This study demonstrates the unique values of multi-sensor RS approaches for mapping and monitoring unregulated gold mining in the Amazon. Across the three AOIs (*Punino*, *Shaime*, and *South Napo*) distinct patterns of mining expansion were observed. *Punino* exhibited rapid, recent intensification along the main river and tributaries beginning in 2023, closely aligning with rising global gold prices. *Shaime*’s subregions displayed heterogeneous dynamics, with some areas peaking in activity around
335 2021-2022 and others, such as *Nangaritza North*, showing steady growth. *South Napo* experienced more gradual expansion, with notable increases after 2021 in both subregions.

The integration of SED, PS, and S-1 SAR datasets allowed both spatial and temporal refinement of mining dynamics. SED provided an accessible, coarse overview of annual trends, while PS enabled higher-resolution mapping and capture of intra-annual variability, based on image availability. S-1-based SCD analysis complemented optical imagery by detecting short-
340 term changes every 12-days, revealing patterns of progressive deforestation and progressive site expansion that optical datasets alone may overlook. The combination of these methods consistently identified deforestation associated with mining, even in remote and inaccessible areas, highlighting the rapid pace and spatial complexity of extractive activity.

Comparisons with independent datasets, including MAAP and the AMW platform, confirm the robustness of the proposed classification framework. Although minor discrepancies arise due to differences in spatial resolution and methodological
345 design, the strong spatial agreement underscores the reliability of the detected trends. Beyond validation, this study demonstrates that combining multiple datasets is an effective approach for capturing both the extent and temporal dynamics of mining, depending on the specific use case. The presented workflows are particularly well suited for integration with platforms such as AMW, enabling more detailed analyses of identified sites and supporting further investigation of mining dynamics.

350 Finally, while these RS approaches effectively map the extent and dynamics of mining, they do not capture the broader ecological and social consequences, including mercury contamination, biodiversity loss, and impacts on Indigenous territories. Integrating RS with in-situ monitoring and interdisciplinary assessments is essential to fully understand the environmental and societal implications of unregulated gold mining in the Amazon.



Code, data, or code and data availability

- 355 All datasets used in this study are publicly available or accessible through research programs. The S-1 data were obtained from the European Space Agency (ESA) and accessed via GEE. The SED was accessed through Google's geospatial data catalogue within GEE. PS imagery was provided through Planet's Education and Research Program and downloaded via the Planet Explorer. The JRC Global Surface Water dataset used for masking permanent water bodies is publicly available within GEE. Outputs from the Amazon Mining Watch platform, are accessible online (<https://amazonminingwatch.org>).
- 360 All data processing and analysis were conducted within GEE using custom scripts. The code used to generate the results of this study is available from the corresponding author upon request.

Author contributions

- IL conducted the conceptualization, methodology development, formal analysis, visualization, and writing of the original draft. VG and CG provided supervision and contributed to reviewing and editing the manuscript, offering critical feedback and
- 365 guidance throughout the study. JJA contributed local expertise and contextual knowledge on Ecuador and supported the interpretation of the results.

Acknowledgments

We acknowledge the contributions of Jan-Erik Feldt for the delineation of the AOI shapefiles. Linguistic improvements were supported by AI-based tools, including DeepL.

370 Competing interests

The authors declare no conflicts of interest.

References

- Abramovay *et al.*, in *Amazon Assessment Report 2021*, C. Nobre *et al.*, Eds. (United Nations Sustainable Development Solutions Network, 2021). <https://doi.org/10.55161/RWSX6527>
- 375 Adamek, K., Lupa, M., & Zawadzki, M. (2021). Remote sensing techniques for tracking changes caused by illegal gold mining in Madre de Dios, Peru. *Miscellanea Geographica. Regional Studies on Development*, 25(4), 205–212. <https://doi.org/10.2478/mgrsd-2020-0028>
- Amazon Mining Watch (2026): <https://amazonminingwatch.org>



- Albert, J. S., Carnaval, A. C., Flantua, S. G., Lohmann, L. G., Ribas, C. C., Riff, D., ... Nobre, C. A. (2023). Human impacts
380 outpace natural processes in the Amazon. *Science*, 379(6630), eabo5003. <https://doi.org/10.1126/science.abo5003>
- Asokan, A., & Anitha, J. J. E. S. I. (2019). Change detection techniques for remote sensing applications: A survey. *Earth
Science Informatics*, 12(2), 143-160. <https://doi.org/10.1007/s12145-019-00380-5>
- Bank, M. S., Vignati, D. A. L., & Vigon, B. (2014). United Nations Environment Programme's Global Mercury Partnership:
Science for successful implementation of the Minamata Convention. *Environmental Toxicology and Chemistry*, 33(6), 1199–
385 1201. <https://doi.org/10.1002/etc.2592>
- Berenguer, E., et al. (2021). In *Amazon Assessment Report 2021* (C. Nobre et al., Eds.). United Nations Sustainable
Development Solutions Network. <https://doi.org/10.55161/RWSX6527>
- Borja, M. O., Aguilar, C., Verdesoto, G., Villa, J., Mamani, N., Finer, M. & C. Josse (2023): MAAP #198: Expansión de la
Minería en la Amazonía de Ecuador. URL: <https://www.maaprogram.org/es/expansion-mineria-ecuador/>
- 390 Breiman, L. (2001). Random forests. *Machine learning*, 45(1), 5-32. <https://doi.org/10.1023/A:1010933404324>
- Brown, C. F., Kazmierski, M. R., Pasquarella, V. J., Rucklidge, W. J., Samsikova, M., Zhang, C., ... Kohli, P. (2025).
AlphaEarth Foundations: An embedding field model for accurate and efficient global mapping from sparse label data. *arXiv*.
<https://doi.org/10.48550/arXiv.2507.22291>
- Canty, M. J., Nielsen, A. A., Conradsen, K., & Skriver, H. (2019). Statistical analysis of changes in Sentinel-1 time series on
395 the Google Earth Engine. *Remote Sensing*, 12(1), 46. <https://doi.org/10.3390/rs12010046>
- Capparelli, M., Cabrera, M., Rico, A., Lucas-Solís, O., Alvear-S., D., Vasco, S., ... Moulatlet, G. M. (2021). An integrative
approach to assess the environmental impacts of gold mining contamination in the Amazon. *Toxics*, 9(7), 149.
<http://dx.doi.org/10.3390/toxics9070149>
- Conradsen, K., Nielsen, A. A., & Skriver, H. (2016). Determining the points of change in time series of polarimetric SAR data.
400 *IEEE Transactions on Geoscience and Remote Sensing*, 54(5), 3007-3024. <https://doi.org/10.1109/TGRS.2015.2510160>
- Cooper, G. S., Willcock, S., & Dearing, J. A. (2020). Regime shifts occur disproportionately faster in larger ecosystems. *Nature
Communications*, 11, 1175. <https://doi.org/10.1038/s41467-020-15029-x>
- Esdaile, L. J., & Chalker, J. M. (2018). The mercury problem in artisanal and small-scale gold mining. *Chemistry—A European
Journal*, 24(27), 6905-6916. <https://doi.org/10.1002/chem.201704840>
- 405 Ferrante, L., & Fearnside, P. M. (2022). Countries should boycott Brazil over export-driven deforestation. *Nature*, 601, 318.
- Flores, B. M., Montoya, E., Sakschewski, B., Nascimento, N., Staal, A., Betts, R. A., ... & Hirota, M. (2024). Critical transitions
in the Amazon forest system. *Nature*, 626(7999), 555-564. <https://doi.org/10.1038/d41586-022-00094-7>
- Forkuor, G., Ullmann, T., & Griesbeck, M. (2020). Mapping and monitoring small-scale mining activities in Ghana using
Sentinel-1 time series (2015–2019). *Remote Sensing*, 12(6), 911. <https://doi.org/10.3390/rs12060911>
- 410 GADM Carlos Julio Arosemena Tola. (2025). *Historia del cantón Carlos Julio Arosemena Tola*.
<https://gadarosemenatola.gob.ec/historia-del-canton/>



- Geudtner, D., Torres, R., Snoeij, P., Davidson, M., & Rommen, B. (2014, July). Sentinel-1 system capabilities and applications. In *2014 IEEE geoscience and remote sensing symposium* (pp. 1457-1460). IEEE. <https://doi.org/10.1109/IGARSS.2014.6946711>
- 415 Gibb, H., & O'Leary, K. G. (2014). Mercury exposure and health impacts among individuals in the artisanal and small-scale gold mining community: a comprehensive review. *Environmental health perspectives*, *122*(7), 667. <https://doi.org/10.1289/ehp.1307864>
- Götze, C., Beyer, F., & Gläßer, C. (2016). Pioneer vegetation as an indicator of the geochemical parameters in abandoned mine sites using hyperspectral airborne data. *Environmental Earth Sciences*, *75*(7), 613. <https://doi.org/10.1007/s12665-016-420-5367-1>
- Graw, V., Dedring, T., Hiby, R., Jara-Alvear, J., Guzman, P., & Juergens, C. (2022). Regressive erosion at river coca in Northeast Ecuador: Landslide monitoring with sentinel-1 to support disaster risk management. *PGF–Journal of Photogrammetry, Remote Sensing and Geoinformation Science*, *90*(5), 457-471. <https://doi.org/10.1007/s41064-022-00221-z>
- 425 Grinand, C., Rakotomalala, F., Gond, V., Vaudry, R., Bernoux, M., & Vieilledent, G. (2013). Estimating deforestation in tropical humid and dry forests in Madagascar from 2000 to 2010 using multi-date Landsat satellite images and the random forests classifier. *Remote Sensing of Environment*, *139*, 68-80. <https://doi.org/10.1016/j.rse.2013.07.008>
- Isidro, C. M., McIntyre, N., Lechner, A. M., & Callow, I. (2017). Applicability of earth observation for identifying small-scale mining footprints in a wet tropical region. *Remote Sensing*, *9*(9), 945. <https://doi.org/10.3390/rs9090945>
- Lenton, T. M., Milkoreit, M., Willcock, S., Abrams, J. F., Armstrong McKay, D. I., Buxton, J. E., ... Dennis, D. (Eds.). (2025). *The Global Tipping Points Report 2025*. University of Exeter.
- 430 Lobo, F. D. L., Souza-Filho, P. W. M., Novo, E. M. L. D. M., Carlos, F. M., & Barbosa, C. C. F. (2018). Mapping mining areas in the Brazilian Amazon using MSI/Sentinel-2 imagery (2017). *Remote Sensing*, *10*(8), 1178. <https://doi.org/10.3390/rs10081178>
- MAAP (2024): MAAP #219: Illegal mining expansion in the Ecuadorian Amazon (Punino area). URL: <https://www.maaprogram.org/maap-219-illegal-mining-expansion-in-the-ecuadorian-amazon-punino-area/>
- 435 MAAP (2025): MAAP #230: Mining in the Ecuadorian Amazon, Central Sector – Napo Province. URL: <https://www.maaprogram.org/ecuador-mining-napo/>
- McFeeters, S. K. (1996). The use of the Normalized Difference Water Index (NDWI) in the delineation of open water features. *International journal of remote sensing*, *17*(7), 1425-1432. <https://doi.org/10.1080/01431169608948714>
- 440 Mena-Quintana, F. N., Álvarez, W., Franco, W., Moncayo, L., Tipán, M., & Ayala, J. (2025). Land Degraded by Gold Mining in the Ecuadorian Amazon: A Proposal for Boosting Ecosystem Restoration Through Induced Revegetation. *Forests*, *16*(2), 372. <https://doi.org/10.3390/f16020372>
- Mora-Silva, D., & Coronel-Espinoza, B. (2021). Minería aurífera artesanal en la Amazonía norte del Ecuador: Gestión e impactos socioambientales en la parroquia El Dorado de Cascales, provincia de Sucumbíos. *Green World Journal*, *4*(3). <https://doi.org/10.53313/gwj42003>
- 445



- Navas, L. O., Robles, P. M., & Mishquero-Ullauri, D. (2020). Conflictos e impactos generados por minería: Una amenaza al territorio de la comunidad indígena Cofán de Sinangoe, Sucumbíos–Ecuador. *Green World Journal*, 3(2), 1–12. <https://doi.org/10.53313/gwj32001>
- Peck, M. R., Desselas, M., Bonilla-Bedoya, S., Redín, G., & Durango-Cordero, J. (2024). The conflict between Rights of Nature and mining in Ecuador: Implications of the Los Cedros Cloud Forest case for biodiversity conservation. *People and Nature*, 6(3), 1096–1115. <https://doi.org/10.1002/pan3.10615>
- Pekel, J. F., Cottam, A., Gorelick, N., & Belward, A. S. (2016). High-resolution mapping of global surface water and its long-term changes. *Nature*, 540(7633), 418–422. <https://doi.org/10.1038/nature20584>
- Phan, T. N., Kuch, V., & Lehnert, L. W. (2020). Land cover classification using Google Earth Engine and random forest classifier—The role of image composition. *Remote Sensing*, 12(15), 2411. <https://doi.org/10.3390/rs12152411>
- Protschky, S., & Morgan, R. A. (2021). Historicising sulfur mining, lime extraction and geotourism in Indonesia and Australia. *The Extractive Industries and Society*, 8(1), 100881. <https://doi.org/10.1016/j.exis.2021.02.001>
- Ramírez Requelme, M. E., Ramos, J. F. F., Angélica, R. S., & Brabo, E. S. (2003). Assessment of Hg-contamination in soils and stream sediments in the mineral district of Nambija, Ecuadorian Amazon. *Applied Geochemistry*, 18(3), 371–381. [https://doi.org/10.1016/S0883-2927\(02\)00088-4](https://doi.org/10.1016/S0883-2927(02)00088-4)
- Rouse, J. W. JR., Haas, R. H., Schell, J. A. & D. W. Deering (1974): Monitoring vegetation systems in the Great Plains with ERST. NASA. Goddard Space Flight Center 3d ERTS-1 Symp., Vol. 1, Sect. A, 309-317
- Roy, B. A., Zorrilla, M., Endara, L., Thomas, D. C., Vandegrift, R., Rubenstein, J. M., ... Read, M. (2018). New mining concessions could severely decrease biodiversity and ecosystem services in Ecuador. *Tropical Conservation Science*, 11, 1940082918780427. <https://doi.org/10.1177/1940082918780427>
- Roy, D. P., Huang, H., Houborg, R., & Martins, V. S. (2021). A global analysis of the temporal availability of PS high spatial resolution multi-spectral imagery. *Remote Sensing of Environment*, 264, 112586. <https://doi.org/10.1016/j.rse.2021.112586>
- Sellers, C., Ammirati, L., Khalili, M. A., Buján, S., Rodas, R. A., & Di Martire, D. (2022). The use of DInSAR techniques for the study of land subsidence associated with illegal mining activities in Zaruma, Ecuador. In *European Workshop on Structural Health Monitoring* (pp. 553–562). Springer. https://doi.org/10.1007/978-3-031-07322-9_56
- United Nations Population Fund (UNFPA) (2025). Ecuador Population 2025 – United Nations Population Fund. <https://www.unfpa.org/data/world-population/EC>.
- Villa, J., Aguilar, C., Villacís, S., Finer, M., & Josse, C. (2022). *Mining activity in the Protective Forest Cuenca Alta del Río Nangaritza (Ecuador)* (MAAP Report No. 167). Monitoring of the Andes Amazon Program.
- Villacis, B., Carrillo, D. *País Atrevido: La Nueva Cara Sociodemográfica del Ecuador*, 1st ed.; Instituto Nacional de Estadística y Censos (INEC): Quito, Ecuador, 2012.
- Wunderling, N., Donges, J. F., Kurths, J., & Winkelmann, R. (2021). Interacting tipping elements increase risk of climate domino effects under global warming. *Earth System Dynamics*, 12, 601–619. <https://doi.org/10.5194/esd-12-601-2021>

<https://doi.org/10.5194/egusphere-2026-1854>

Preprint. Discussion started: 10 April 2026

© Author(s) 2026. CC BY 4.0 License.



480 Zhang, B., Wu, D., Zhang, L., Jiao, Q., & Li, Q. (2012). Application of hyperspectral remote sensing for environment
monitoring in mining areas. *Environmental Earth Sciences*, 65(3), 649–658. <https://doi.org/10.1007/s12665-011-1112-y>